Efficient 5.2 μm wavelength fiber-to-chip grating couplers for the Ge-on-Si and Ge-on-SOI mid-infrared waveguide platform

Sanja Radosavljevic, Bart Kuyken and Gunther Roelkens

Photonics Research Group, Ghent University - imec, Technologiepark 15, 9052 Ghent, Belgium

Center for Nano- and Biophotonics, Technologiepark 15, 9052 Ghent, Belgium

sanja.radosavljevic@ugent.be

Abstract: We present the design, fabrication and characterization of efficient fiber-to-chip grating couplers on a Germanium-on-Silicon (Ge-on-Si) and Germanium-on-silicon-on-insulator (Ge-on-SOI) platform in the 5 μm wavelength range. The best grating couplers on Ge-on-Si and Ge-on-SOI have simulated coupling efficiencies of -4 dB (40%) with a 3 dB bandwidth of 180 nm and -1.5 dB (70%) with a 3 dB bandwidth of 200 nm, respectively. Experimentally, we show a maximum efficiency of -5 dB (32%) and a 3 dB bandwidth of 100 nm for Ge-on-Si grating couplers, and a -4 dB (40%) efficiency with a 3 dB bandwidth of 180 nm for Ge-on-SOI couplers.

OCIS codes: (050.2770) Gratings, (130.3120) Integrated optics devices.

References and links

1. P.A. Werle, "Review of recent advances in semiconductor laser based gas monitors", *Spectrochim. Acta Mol. Biomol. Spectrosc.* **54**(2), 197–236 (1998).
2. J. Hodgkinson, and R.P. Tatam, "Optical gas sensing : a review", *Meas. Sci. Technol.* **24**(1), 012004 (2012).
3. M. Nedeljkovic, A.V. Velasco, A.Z. Khokhar, A. Delge, P. Cheben, and G.Z. Mashanovich, "Mid-infrared silicon-on-insulator Fourier-transform spectrometer chip", *IEEE Photon. Technol. Lett.* **28**(4), 528–531 (2016).
4. F. Adler, P. Masowski, A. Foltynowicz, K.C. Cossel, T.C. Briles, I. Hartl, and J. Ye, "Mid-infrared Fourier transform spectroscopy with a broadband frequency comb", *Opt. Express*, **18**(21), 21861–21872 (2010).
5. Z. Cheng, X. Chen, C.Y. Wong, K. Xu, and H.K. Tsang, "Mid-infrared suspended membrane waveguide and ring resonator on silicon-on-insulator", *IEEE Photon. J.* **4**(5), 1510–1519 (2012).
6. T. Baehr-Jones, A. Spott, R. Ilic, A. Spott, B. Penkov, W. Asher, and M. Hochberg, "Silicon-on-sapphire integrated waveguides for the mid-infrared", *Opt. Express*, **18**(12), 12127–12135 (2010).
7. J.M. Ramirez, V. Vakarin, C. Gilles, J. Frigerio, A. Ballabio, P. Chaisakul, X. Le Roux, C. Alonso-Ramos, G. Maisons, L. Vivien, M. Carras, G. Isella, and D. Marris-Morini, "Low-loss Ge-rich $Si_{0.2}Ge_{0.8}$ waveguides for mid-infrared photonics", *Opt. Lett.* **42**(1), 105–108 (2017).
8. L. Carletti, M. Sinobad, P. Ma, Y. Yu, D. Allioux, R. Orobtchouk, M. Brun, S. Ortiz, P. Labeye, J. M. Hartmann, S. Nicoletti, S. Madden, B. Luther-Davies, D. J. Moss, C. Monat, and C. Grillet, "Mid-Infrared nonlinear optical response of Si-Ge waveguides with ultra-short optical pulses", *Opt. Express*, **23**(25), 32202–32214 (2015).
9. R.A. Soref, "Mid-infrared photonics in silicon and germanium", *Nat. Photon*, **4**(8), 495–497 (2010).
10. A. Malik, M. Muneeb, S. Radosavljevic, M. Nedeljkovic, J.S. Penades, G. Mashanovich, Y. Shimura, G. Lepage, P. Verheyen, W. Vanherle, and T. Van Opstal, "Ge-on-Si and Ge-on-SOI thermo-optic phase shifters for the mid-infrared", *Opt. Express*, **22**(23), 28479–28488 (2014).
11. A. Malik, M. Muneeb, S. Pathak, Y. Shimura, J. Van Campenhout, R. Loo, and G. Roelkens, "Germanium-on-silicon mid-infrared arrayed waveguide grating multiplexers", *IEEE Photon. Technol. Lett.* **25**(18), 1805–1808 (2013).

12. A. Malik, M. Muneeb, Y. Shimura, J. Van Campenhout, R. Loo, and G. Roelkens, "Germanium-on-silicon planar concave grating wavelength (de)multiplexers in the mid-infrared," *Appl. Phys. Lett.* **103**(16), 161119 (2013).
13. P. Barritault, M. Brun, P. Labeye, J. Hartmann, F. Boulila, M. Carras, and S. Nicoletti, "Design, fabrication and characterization of an AWG at 4.5 μm" *Opt. Express*, **23**(20), 26168–26181 (2015).
14. A. Koshkinbayeva, P. Barritault, S. Ortiz, S. Boutami, M. Brun, J. Hartmann, P. Brianceau, O. Lartigue, F. Boulila, R. Orobtchouk, and P. Labeye, "Impact of non-central input in NM mid-IR arrayed waveguide gratings integrated on Si" *IEEE Photon. Technol. Lett.* **28**(20), 2191–2194 (2016).
15. S. Radosavljevic, B. Kuyken and G, Roelkens, "A fiber-to-chip grating goupler for the Ge-on-Si platform at 5 μm wavelength", *ECIO Proceedings* (to be published).
16. M. Nedeljkovic, J.S. Penads, C.J. Mitchell, A.Z. Khokhar, S. Stankovic, T.D. Bucio, C.G. Littlejohns, F.Y. Gardes, and G.Z. Mashanovich, "Surface-grating-coupled low-loss Ge-on-Si rib waveguides and multimode interferometers", *IEEE Photon. Technol. Lett.* **27**(10), 1040–1043 (2015).
17. C. Alonso-Ramos, M. Nedeljkovic, D. Benedikovic, J.S. Penads, C.G. Littlejohns, A.Z. Khokhar, D. Prez-Galacho, L. Vivien, P. Cheben, and G.Z. Mashanovich, "Germanium-on-silicon mid-infrared grating couplers with low-reflectivity inverse taper excitation", *Opt. Lett.* **41**(18), 4324–4327 (2016).
18. J. Favreau, C. Durantin, J. Fdli, S. Boutami, and G. Duan, "Suspended mid-infrared fiber-to-chip grating couplers for SiGe waveguides", *Proc. SPIE 9753, Optical Interconnects XVI*, 975319–975319 (2016).
19. Z. Cheng, X. Chen, C. Y. Wong, K.X. Christy, K.Y. Fung, Y.M. Chen, and H.K. Tsang, "Mid-infrared grating couplers for Silicon-on-Sapphire waveguides", *IEEE Photon. J.* **4**(1), 104–113 (2012).
20. M. Brun, P. Labeye, G. Grand, J. Hartmann, F. Boulila, M. Carras, and S. Nicoletti, "Low loss SiGe graded index waveguides for mid-IR applications", *Opt. Express*, **22**(1), 508–518 (2014).
21. B. Troia, J.S. Penades, A.Z. Khokhar, M. Nedeljkovic, C. Alonso-Ramos, and V.M. Passaro, G.Z. Mashanovich, "Germanium-on-silicon Vernier-effect photonic microcavities for the mid-infrared", *Opt. Lett.* **41**(3), 610–613 (2016).
22. B. Troia, A.Z. Khokhar, M. Nedeljkovic, J.S. Penades,V.M. Passaro, and G.Z. Mashanovich, "Cascade-coupled racetrack resonators based on the Vernier effect in the mid-infrared", *Opt. Lett.* **22**(20), 23990–24003 (2014).
23. R. Shankar, I. Bulu, and M. Lonar, "Integrated high-quality factor silicon-on-sapphire ring resonators for the mid-infrared", *Appl. Phys. Lett.* **102**(5), 051108 (2013).
24. A. Spott, J. Peters, M.L. Davenport, E.J. Stanton, C.D. Merritt, W.W. Bewley, I. Vurgaftman, C.S. Kim, J.R. Meyer, J. Kirch, and L.J. Mawst, "Quantum cascade laser on silicon", *Optica*, **3**(5), 545–551 (2016).
25. B. Wang, J.H. Jiang, and G.P. Nordin, "Embedded, slanted grating for vertical coupling between fibers and silicon-on-insulator planar waveguides", *IEEE Photon. Technol. Lett.* **17**(9), 1884–1886 (2005).
26. F. Van Laere, G. Roelkens, M. Ayre, J. Schrauwen, D. Taillaert, D. Van Thourhout, T. F. Krauss, and R. Baets, "Compact and highly efficient grating couplers between optical fiber and nanophotonic waveguides", *J. Lightwave Technol.* **25**(1), 151–156 (2007).
27. D. Vermeulen, S. Selvaraja, P. Verheyen, G. Lepage, W. Bogaerts, P. Absil, D. Van Thourhout, and G. Roelkens, "High-efficiency fiber-to-chip grating couplers realized using an advanced CMOS-compatible Silicon-On-Insulator platform", *Opt. Express* **18**(17), 18278–18283 (2010).
28. X. Chen, C. Li, C.K.Y. Fung, S.M.G. Lo, and H.K. Tsang, "Apodized waveguide grating couplers for efficient coupling to optical fibers", *IEEE Photon. Technol. Lett.* **22**(15), 11561158 (2010).
29. M. Antelius, K.B. Gylfason, and H. Sohlstrm, "An apodized SOI waveguide-to-fiber surface grating coupler for single lithography silicon photonics", *Opt. Express*, **19**(4), 35923598 (2011).
30. C. Li, H. Zhang, M. Yu, and G.Q. Lo, "CMOS-compatible high efficiency double-etched apodized waveguide grating coupler", *Opt. Express*, **21**(7), 7868–7874 (2013).
31. http://www.spectralcalc.com/spectral_browser/db_intensity.php
32. https://www.thorlabs.com/newgrouppage9.cfm?objectgroupid=7999

1. Introduction

Besides the traditional applications of telecom and datacom, integrated photonics finds its use in other fields, such as optical gas sensing, which is a vital element in several industrial, medical and environmental applications. The mid-infrared (midIR) wavelength range is of particular interest for these applications due to the orders of magnitude higher optical absorption cross-section in this range as compared to the telecom and visible wavelength range [1–4]. Up to this point multiple platforms have been suggested for the implementation of midIR photonic integrated circuits (PICs), some of which are suspended Si membrane [5], silicon-on-sapphire (SOS) [6] and graded index GeSi platform [7] which also finds its application in non-linear photonics [8]. While bulk Si is considered transparent only up to 8 μm wavelength, Ge has low losses in the 2-14 μm wavelength range [9], which - together with its compatibility with

standard CMOS/MEMS processes - makes it suitable for the implementation of midIR gas sensor PICs for this wavelength range. Recently, Ge-on-Si and Ge-on-SOI have emerged as platforms for sensing applications beyond 4 μm wavelength [9]. The Ge-on-Si platform has the advantage over the other mid-IR platforms of simple fabrication and wider transparency window. Unlike the Ge-on-Si platform, the Ge-on-SOI stack has an extra SiO_2 layer which allows for more efficient integrated heaters [10]. Fabrication of devices on this platform can take advantage of this SiO_2 layer to perform under-etching step on parts of the PIC. In contrast to suspended Si platform, only certain parts of PICs that necessitate under-etching to enhance their performance, such as gratings and heaters, would be suspended in air which makes this platform more robust and also enables implementation of larger devices that would otherwise be difficult to suspend entirely, for instance arrayed waveguide gratings (AWGs) and planar concave gratings (PCGs).

Considerable research is geared towards the integration and miniaturization of various optical components for the midIR on these platforms, such as AWGs and PCGs [11–14], grating couplers and low loss waveguides [6, 15–20], ring resonators [12, 21, 22] and quantum cascade laser (QCL) source integration [24]. Packaging, as well as wafer-level testing of these optical devices requires the implementation of efficient fiber-to-chip grating couplers.

The efficiency of a grating coupler is limited by its directionality (power difracted towards the fiber with respect to power in the waveguide) and the overlap between a fiber mode and the field difracted by the grating towards the fiber. Many approaches have been suggested to improve the directionality, especially on telecommunication wavelength range, such as slanted gratings [25], a substrate mirror [26] or a silicon overlay [27]. The fabrication of the slanted gratings or substrate mirror is not CMOS compatible and it is very complex, while the use of amorphous silicon limits the thermal budget. Other designs yielded equally efficient grating couplers due to optimization of the overlap between the fiber mode and scattered field of the grating [28–30]. However, experimentally characterized grating couplers in the mid-IR have proven to have lower efficiency then the couplers at telecom wavelength range [17–19].

In [15] we report our first results on Ge-on-Si grating couplers for the 5 μm wavelength range. In this paper we elaborate on the design, fabrication and characterization of the devices. We also present high-efficiency grating coupler on the Ge-on-SOI platform. As the vision is that these PICs will be butt-coupled to a QCL emitting TM polarized light, our couplers are optimized for TM polarization. We focus our work on the wavelength range of our QCL, the 5.15-4.45 μm wavelength range. In this wavelength region we can find absorption lines of acetylene, formic acid, ammonia and many other compounds of interest [31].

2. Coupler Design and Measurements

2.1. High-level overview of the grating coupler designs

The schematic cross-sections of the grating structures designed on the Ge-on-Si and Ge-on-SOI platform are shown in Fig. 1a and b, respectively. For the Ge-on-Si platform we use a standard second order grating structure with a uniform grating period and duty cycle. For the Ge-on-SOI platform we have designed a more complex grating structure to optimize the coupling efficiency. In fact, a fourth order grating is used, comprising of a uniform and apodized grating section. Secondly, the SiO_2 layer is locally removed to enhance the coupling efficiency further, as the reflectivity of the Si/air interface is larger than the reflectivity of the Si/SiO_2 interface.

The wave-vector diagrams for both cases assuming a uniform grating are shown in Fig. 2. The Si bottom cladding supports the propagation of several diffraction orders for the fourth order grating. Generally, for the same layer stack, it is expected that second order gratings exhibit higher coupling efficiency than fourth order gratings due to the larger number of diffraction orders in the latter case. However, at the Si/air interface these higher diffraction orders undergo

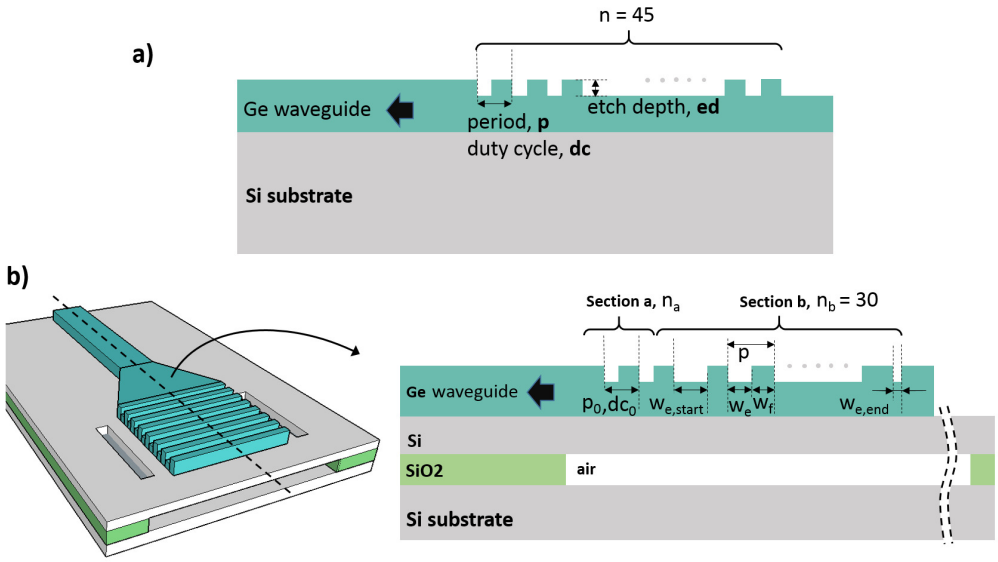

Fig. 1. Schematic of the grating structures designed on the Ge-on-Si (a) and Ge-on-SOI (b) waveguide platform

total internal reflection - as indicated in Fig. 2 b) by the blue circle representing the length of the k-vectors in air - whereby they are 'recycled' in the structure. This results in only a single diffraction order propagating in the air gap towards the silicon substrate. By properly optimizing the layer structure the power in this downwards diffracted field can be minimized, thereby maximizing the directionality of the grating structure towards the optical fiber. Note that the total reflectivity of the substrate comprises the coherent addition of a reflection at the Si-air and air-Si substrate interface, therefore the buried oxide layer thickness also has an impact in the case of the Ge-on-SOI coupler. To further increase the fiber coupling efficiency we implemented an apodization where the etched feature w_e changes linearly from $w_{e,start}$ to $w_{e,end}$ and where w_f is determined by:

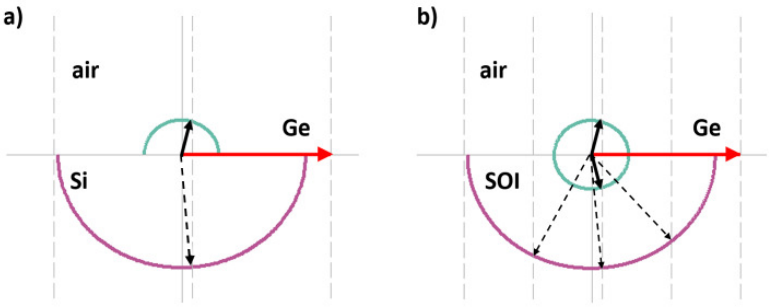

Fig. 2. Vector diagram of a second order Ge-on-Si grating (a) and a fourth order Ge-on-SOI grating (b) with the buried oxide layer locally removed. The allowed diffraction orders in air (solid arrows) and Si under-cladding (dashed arrows) are also indicated

$$p(n_e + n_f)/2 = w_e n_e + w_f n_f \quad (1)$$

where p is the period of the corresponding grating coupler with the same etch depth when the duty cycle is constant and equal to 0.5, optimized for a given fiber angle. w_e and n_e are the width of the slit and the effective index of the fundamental TM mode in the slit respectively, while w_f and n_f are the width of the unetched part and effective index of the fundamental TM mode of the unetched part of the grating respectively. Another feature of the grating is that it has n_a grooves at the entrance of the grating coupler structure with uniform duty cycle dc_0 and period p_0, which makes the perturbation of the waveguide caused by the grating less abrupt and reduces reflection in the waveguide when coupling from the PIC to the fiber. This section is marked as section A in Fig. 1. The sections A and B are designed with the same etch depth. The proposed design is a trade-off between the complexity of the grating structure, both in terms of device optimization and fabrication, and the fiber-to-chip coupling efficiency. The parameters are optimized for maximal efficiency at a wavelength of 5.2 μm.

2.2. *Measurement setup*

The measurement setup is schematically shown in Fig. 3. Light from the free-space emitting external cavity QCL (Daylight solutions) operating in continuous wave (CW) is coupled to an InF single mode fiber with a mode field diameter of 17 μm at 5.2 μm wavelength. Between the laser and the fiber coupler we have a Babinet-Soleil polarization control element and a chopper.

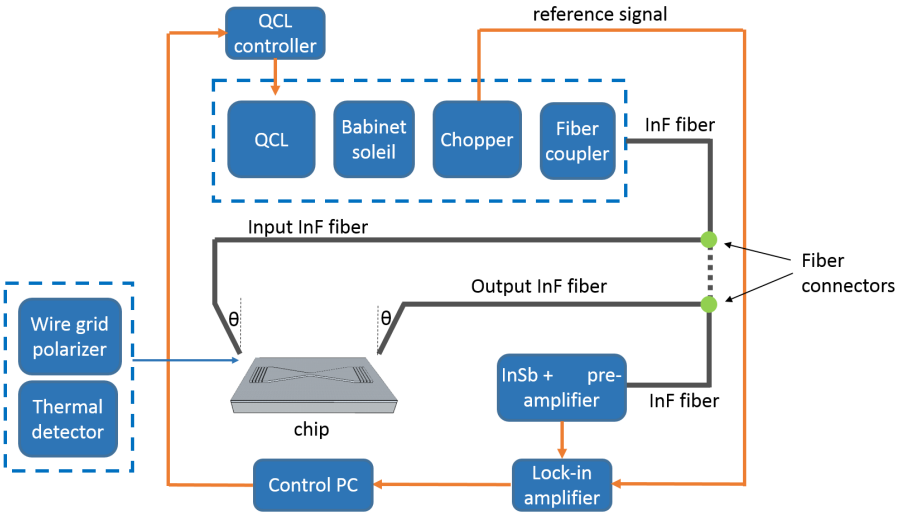

Fig. 3. The measurement setup. A control PC sets the wavelength of the QCL in CW mode through the QCL controller. The light from the laser goes through the Babinet-Soleil polarization control element and the chopper that turns the QCL output into a 50% pulsed signal which is then coupled to the single mode InF fiber by a chalcogenide objective lens. The device transmission is measured by a pre-amplified InSb detector and a lock-in amplifier that receives the reference from the chopper and sends the detected signal back to the control PC. A wire grid polarizer and a thermal detector are used to determine the fraction of light in the TM polarization at the input of the grating. The QCL power is measured on the InSb detector, by connecting directly the two fiber connectors - dashed grey line on diagram

The chopper turns the CW light into 50% duty cycle pulses and hence allows us to detect the signal using a pre-amplified InSb detector and a lock-in amplifier. With the polarization control element we maximize the transmission through the device at the central wavelength. This way we ensure that most of the light is TM polarized at the output facet of the fiber, as the gratings are optimized for TM polarization. Since the fibers are not polarization maintaining we measured the TM fraction of light R_{TM} as a function of wavelength at the output facet of the input fiber by placing a wire grid polarizer and a thermal detector under the fiber facet. The fact that the light is not perfectly linearly polarized across the wavelength range of interest is taken into account in the calculation of the coupling efficiency. The loss caused by the difference in length of the fiber when measuring the transmission through the chip (full grey line in Fig. 3) and when measuring the QCL power P_{QCL} directly (dashed grey line in Fig. 3) is not negligible in the wavelength range of interest and is evaluated from [32]. The fiber loss ranges from 1-2.5 dB/m over the considered wavelength range. Taking all of this into account, the efficiency $\eta(\lambda)$ of a single fiber-to-chip grating coupler is given by

$$\eta(\lambda)[dB] = 10log_{10}\frac{P_{trans}(\lambda)}{P_{QCL}(\lambda)R_{TM}(\lambda)} + A_{fiber}(\lambda)[dB] + 3dB \tag{2}$$

where $P_{trans}(\lambda)$ is the power received by the detector when coupled through the chip, $A_{fiber}(\lambda)$ is the attenuation caused by the difference in fiber length mentioned earlier, and the 3 dB comes from the fact that we measure the transmission through two couplers.

2.3. Grating Coupler for the Ge-on-Si platform

When designing a uniform second order grating coupler for the Ge-on-Si platform, we optimized the period of the grating to ensure that maximal coupling is achieved at the central wavelength of interest. We additionally optimized the duty cycle and the etch depth of the grat-

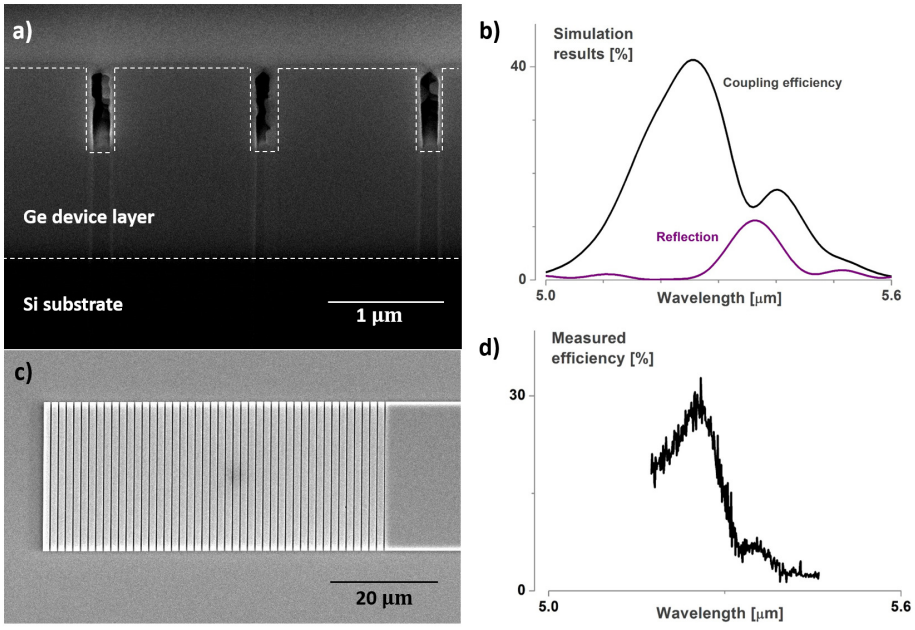

Fig. 4. Cross-section (a) and top view of the optimized Ge-on-Si grating coupler (c). Simulation (b) and measured data of the same device (d).

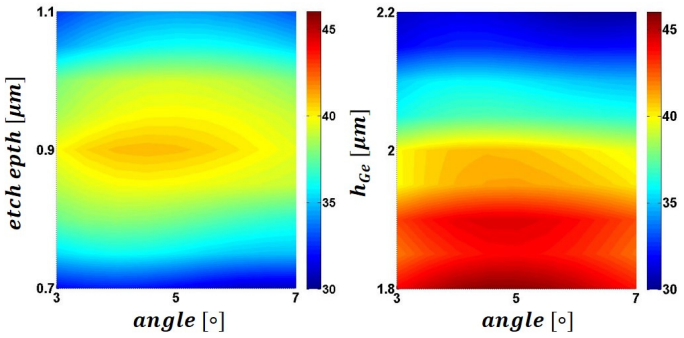

Fig. 5. Maximum coupling efficiency in the 5-5.6 μm wavelength range for the Ge-on-Si grating coupler as a function of the grating etch depth and fiber angle (a) and as a function of thickness of the Ge layer and fiber angle (b)

ings to achieve the best directionality of our structure and maximum overlap of the diffracted field profile with the fiber mode. Other parameters taken into consideration are the angle between the fiber and the vertical y-axis, and the position of the fiber on the x-axis parallel to the grating. The number of grooves was kept constant at 30. All simulations were performed using a 2D finite-difference-time-domain solver. The best simulated TM coupler for Ge-on-Si with 2 μm thick Ge device layer, has a period of 1.45 μm and an etch depth of 0.9 μm with a duty cycle of 0.8 (defined as the width of the unetched Ge grating teeth and the grating period). The optimal fiber angle for the coupler is 5^o. A maximum coupling efficiency of 40% with a 3 dB bandwidth of 180 nm is obtained (see the top graph in Fig. 4(b)). The best lateral overlap of the fiber mode and the fundamental TM grating mode was achieved for a 27.5 μm wide grating.

A cross-section and top-view picture of the realized grating coupler structures is shown in Fig. 4(a). The couplers, together with the waveguides, were etched in one step by a CF_4/H_2 plasma using a titanium/chromium mask. The mask was defined by e-beam lithography using a positive resist and lift-off process. After the etching process the metal mask was removed by HF wet etching.

Experimentally, a fiber-to-chip coupling efficiency of 30% and a 3dB bandwidth of about 100 nm is obtained (see the bottom graph in Fig. 4(b)). In Fig. 5 we show the impact of the grating etch depth and germanium waveguide layer thickness on the fiber coupling efficiency, as a function of the fiber-to-chip grating angle. By varying the etch depth or the Ge thickness within $\pm$100 nm of the optimal value we lose less than 5% in maximum coupling efficiency which means that our design has high tolerance to fabrication imperfections.

2.4. Grating Coupler for the Ge-on-SOI platform

In our Ge-on-SOI design we have fixed the thicknesses of the Ge layer to 2 μm. The SiO_2 layer was also fixed to 2 μm, because of the commercial availability of such SOI wafers. The thickness of the Si layer is to be optimized such that we maximize the directionality of the grating, as discussed above. However, the Si layer has to be thicker than 3 μm so that the loss of the optical mode is not enhanced by the overlap with the SiO_2 layer, which is heavily absorbing in the wavelength range of interest. The optimized coupler has a period of $p = 2.88$ μm, an etch depth of $h = 0.5$ μm, with $w_{e,start} = 1.4$ μm and $w_{e,end} = 0.5$ μm. *Section a* has $n_a = 2$, a period of $p_0 = 1.8$ μm and a duty cycle of $dc_0 = 0.5$. The thickness of the Si layer in this case is 3.2 μm. The angle of the fiber is 10^o. The Ge-on-SOI coupler with these parameters has a simulated coupling efficiency of about 70% and a 3dB bandwidth of 200 nm, as shown in

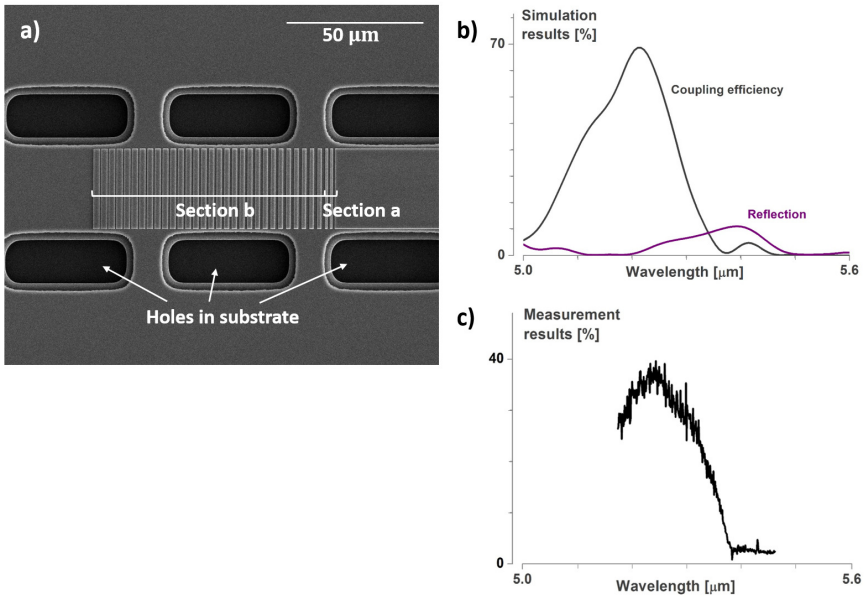

Fig. 6. SEM image of the locally free-standing Ge-on-SOI grating coupler (a). Simulation (b) and measured data of the same device (c).

the top graph of Fig. 6(b).

A top-view image and schematic view of the fabricated grating coupler structure is shown in Fig. 6(a). We have locally under-etched the grating by accessing the SiO_2 layer through narrow openings in the Si layer and by HF wet etching of the oxide layer. The rest of the SiO_2 layer serves as support such that the free-standing structures would not collapse. The couplers, together with the waveguides, were etched in one step by CF_4/H_2 plasma using a titanium/chromium mask. The mask was defined by e-beam lithography using a positive resist and lift-off process. After the etching process the mask was removed by HF wet etching.

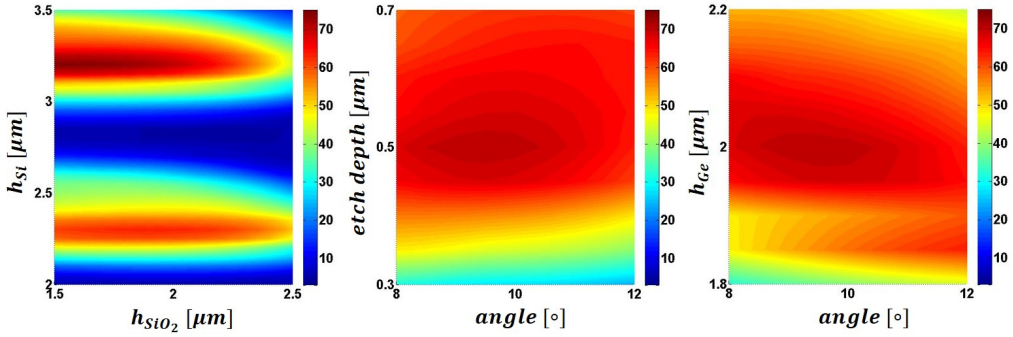

Fig. 7. Maximum fiber-to-chip coupling efficiency in the 5 to 5.6 μm wavelength range for the Ge-on-SOI grating coupler depending on different parameters: Si and SiO_2 layer thickness (a), grating etch depth and fiber angle (b) and the thickness of the Ge waveguide layer vs. fiber angle (c)

The measured device has a maximum efficiency of 40% and a 3 dB bandwidth of 180 nm estimated by interpolation (Fig. 6(c)). In Fig. 7 we show the dependence of the maximum coupling efficiency on different parameters (the thickness of the silicon cladding h_{Si}, the thickness of the buried oxide layer h_{SiO_2}, the thickness of the Ge waveguide layer and the grating etch depth). Due to the interference mechanism in the layers under the grating, efficiency strongly depends on the layer thicknesses in the substrate. Up to 10% can be lost in maximum coupling efficiency by varying the thicknesses of the Ge or Si layer within $\pm$50 nm of the optimal value. The insertion loss is dependent on the thickness of the SiO_2 layer - by changing the thickness of this layer by $\pm$100 nm we can lose up to 5% in maximum coupling efficiency. The difference in the maximum simulated and measured efficiency is attributed to the fabrication imperfections. Comparing to the Ge-on-Si design, this coupler is less tolerant to fabrication imperfections, as it has more parameters whose small variations can contribute to a decrease in the peak efficiency.

3. Conclusion

We have reported efficient Ge-on-Si and Ge-on-SOI grating couplers for the 5μm wavelength range. According to our simulations, the best uniform TM grating couplers for the Ge-on-Si waveguide platform have a coupling efficiency of 40% with a 3dB bandwidth of 180 nm. A reasonable match with the measured device with 30% maximum efficiency and a 100 nm 3 dB bandwidth is obtained. The best simulated locally free-standing grating coupler for the Ge-on-SOI platform has a coupling efficiency of 70% and a 3dB bandwidth of 200 nm, while the fabricated device has a maximum efficiency of 40% and an estimated 3dB bandwidth of 180 nm. These structures will enable the wafer-scale testing of mid-infrared photonic integrated devices realized on a wafer-scale. The high performance on the Ge-on-SOI waveguide platform is particularly interesting, as the buried oxide layer also allows the integration of efficient thermo-optic tuning elements on the platform as described in [10]. This waveguide platform can enable next generation mid-infrared photonic integrated circuits for applications in spectroscopic sensing.

Acknowledgment
The authors would like to acknowledge Dr. ir. Yanlu Li for fruitful discussions and assistance with design optimization.